Measurement of the Level Shift in He^+, $n = 3$*

D. L. Mader,† M. Leventhal,‡ and W. E. Lamb, Jr.
Physics Department, Yale University, New Haven, Connecticut 06520
(Received 12 November 1970)

The level shift δ ($^2S_{1/2}$-$^2P_{1/2}$) and the fine-structure interval $\Delta E - \delta$($^2S_{1/2}$-$^2P_{3/2}$) have been measured in the $n=3$ level of the helium ion He^+ with a microwave-optical technique. Electron bombardment of helium gas produces excited ions. The 1640-Å light from the $n=3$ to 2 decay undergoes a decrease when a microwave field induces an S-to-P transition. Extensive data were taken on three transitions as a function of microwave power, helium pressure, and bombarding current in a search for systematic effects. The major effect was a slight shift of the resonance curves with microwave power due to transitions in higher excited states. The high-frequency transitions αc and βd yield $\Delta E - \delta = 47\,844.05 \pm 0.48$ MHz. Using the Taylor, Parker, and Langenberg value for the fine-structure constant to calculate ΔE, we obtain an indirect measurement of $\delta = 4183.73 \pm 0.51$ MHz. Measurements on αe yield a direct value of $\delta = 4183.17 \pm 0.54$ MHz, which, combined with the indirect value, yields $\delta = 4183.45 \pm 0.52$ MHz, in agreement with the theoretical value of 4184.4 ± 0.5 MHz of Applequist and Brodsky. (All uncertainties are expressed as 68% confidence values.)

I. INTRODUCTION

The level shift δ ($^2S_{1/2}$-$^2P_{1/2}$) and the fine-structure interval $\Delta E - \delta$ ($^2S_{1/2}$-$^2P_{3/2}$) have been measured in the $n=3$ level of the helium ion He^+ to a precision of one part per thousand of the linewidth. The result for $\Delta E - \delta$ can be converted into an indirect measurement of δ if one adopts a value for α, the fine-structure constant, in order to calculate ΔE. Using the Taylor-Parker-Langenberg (TPL)[1] value of α, the direct and indirect measurements of δ agree with each other and also with the current theoretical result of Applequist and Brodsky[2] to an accuracy of 0.02%.

Early measurements[3] on this level using optical spectroscopy agreed with theory and by 1950 had attained an accuracy of 3%. In the $n=2$ level of He^+, δ was measured by Lamb and Skinner[4] using a microwave-optical technique. This measurement was done to high precision by Lipworth and Novick[5] and by Narasimham.[6]

A preliminary measurement of $\delta = 4183 \pm 20$ MHz in $n=3$ of He^+ was made by Leventhal, Lea, and Lamb.[7] A higher-precision result of 4181.9 MHz superseded by this paper was quoted to ±1.0 MHz by Mader and Leventhal.[8] The report[9] of the same authors on $\Delta E - \delta$ is essentially unchanged in this paper.

The motivation for this experiment was the possibility of making a high-precision measurement in order to test the Z and n dependences of the quantum electrodynamical calculation of the level shift. An experimental simplification for $n=3$ arises from the steady-state nature of the problem due to short lifetimes, whereas in $n=2$ the motion of the metastable S ions is a complication. For a given level, an advantage of He^+ over hydrogen is a reduction in the ratio of Stark shifts to fine-structure intervals by a factor of 700 (at zero magnetic field).

In the microwave-optical technique, one observes a change in light emitted by the atoms in order to detect a microwave-induced transition between, say, an S and a P state. According to the analysis of Lamb and Sanders,[10] a nonvanishing signal requires that the branching ratios for optical decay of the two states, as well as their unperturbed steady-state populations, must be different. The first condition is easily met in the present case, and the second is likely to be met since the decay rate for P states is 30 times that of S states.

In this experiment, helium gas is bombarded in an electron beam to form excited ions. The interaction region for the helium, electrons, microwaves, and a magnetic field is the interior of a perforated section of waveguide situated between the poles of a magnet. When the magnetic field is swept across a wide range, the 1640-Å light flux exhibits resonances as the Zeeman effect brings the various electric dipole transition frequencies into coincidence with the fixed microwave frequency.

Enough data were taken on each of the transitions αe, αc, and βd to permit a search for variations of results with microwave power, helium pressure, and bombarding current. The raw values of $\Delta E - \delta$ obtained from βd showed pressure and current shifts due to the coupling of β and f in collisions with atoms and ions. Corresponding results obtained from αe and αc show no significant pressure or current shifts, but do depend on microwave power. An extrapolation formula is used to extract a final result from the raw measurements.

Additional information on this apparatus can be found in papers[11] dealing with other states of H and He^+.

II. THEORY

A. Energy Levels for $n = 3$

The fine structure of the $n = 3$ level shown in Fig. 1 is characterized by four energy level separations: ΔE, $\$$, $\mathfrak{D}\mathcal{S}$, and Σ. The contributions of several authors to the calculation of the level shift $\$$ have been compiled by Erickson and Yennie.[12] Erickson has provided the values shown in Table I for ΔE and $\$$ in the He^+ $n = 3$ case.[13] The remaining two separations were calculated using simple formulas for the Dirac splitting, second-order radiative shift, and anomalous magnetic moment.[14] During the course of this experiment, a new value[1] for α, the fine-structure constant, has been established and a new calculation[2] of $\$$ has been made. Since we use the Erickson values of ΔE and $\$$ in the Hamiltonian, the corrections we find are corrections to the "old" fine-structure calculations. However, when discussing the possibility of a discrepancy between experiment and theory we consider the new values in Sec. IV H.

B. Energy Levels in a Magnetic Field

The fine-structure magnetic sublevels are split by application of a magnetic field. An effective Hamiltonian[10] may be written for each value of l. Writing the magnetic interaction as $\mathfrak{M}$ we have the following Hamiltonians for S, P, and D states:

$$\mathcal{H}_S = \$ + \mathfrak{M}, \quad \mathcal{H}_P = \tfrac{2}{3}\Delta E(1 + \vec{L}\cdot\vec{S}) + \mathfrak{M},$$
$$\mathcal{H}_D = \Delta E + \Sigma + \tfrac{2}{5}\mathfrak{D}\mathcal{S}\,(\tfrac{3}{2} + \vec{L}\cdot\vec{S}) + \mathfrak{M}, \tag{1}$$

where

$$\mathfrak{M} = g_s\mu_B\vec{S}\cdot\vec{H} + g_l\mu_B\vec{L}\cdot\vec{H}\ .$$

The evaluation of $\mu_B H$ is discussed in Sec. III A.

Basis vectors in the "high-field" (l, m_l, m_s) representation were chosen for evaluation of the elements in the Hamiltonian matrix, shown in Fig. 2. Off-diagonal elements arise from the "spin-orbit" interaction $(\vec{L}\cdot\vec{S})$ and cause mixing of the basis vectors. For a given magnetic field, the Hamiltonian matrix was evaluated and then diagonalized to obtain energy levels and eigenstates. In Table II, the 18 eigenstates, named according to the nomenclature of Lamb and Sanders,[10] are identified in the high-field limit. At intermediate fields there are 44 electric dipole transitions between these eigenstates. Electric dipole matrix elements for the coupling of two levels were computed as a field-dependent linear combination of the high-field electric dipole matrix elements. Stark shifts were calculated as the change in transition frequencies upon assigning nonzero values to E_x or E_z (see Fig. 2) in the Hamiltonian.

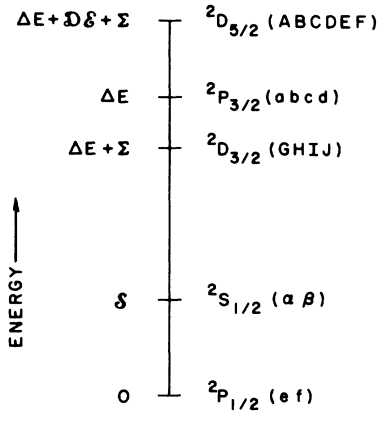

FIG. 1. Fine structure of $n = 3$. Sublevels belonging to each fine-structure level are shown in order of decreasing magnetic quantum number. Levels are not drawn to scale.

TABLE I. Physical constants used in the Hamiltonian. The fine-structure separations $\$$ and ΔE are old values based on $\alpha^{-1} = 137.03876$ and a fourth-order contribution to $\$$ calculated by Soto. Experimental corrections Δ to these theoretical values of $\$$ or $\Delta E - \$$ were found. The uncertainty in $\$$ is $\frac{1}{3}$ of Erickson's "limit of error."

Symbol	Value	Reference
$\$$	4182.43 ± 0.41 MHz	13
ΔE	52025.71 ± 0.14 MHz	13
$\mathfrak{D}\mathcal{S}$	17300 MHz	
Σ	−85 MHz	
g_s	2.002319124 ± 0.000000054	15
g_l[a]	0.999862903 ± 0.000000010	16
g_J/g_W	658.21591 ± 0.00002	17

[a] $g_l = 1 - m_e/M_a$.

C. Selection of Transitions

The transition frequency diagram, Fig. 3, shows the ten S-to-P electric dipole transitions. Dashed lines represent π-polarized transitions which have $\Delta m = 0$ and are driven by an electric field parallel to the magnetic field. The solid lines show σ-polarized transitions ($\Delta m = \pm 1$) which require an electric field transverse to the magnetic field. The electron cyclotron resonance is also shown. Since the microwave field was established in a waveguide, transitions of a given polarization could be selected with the appropriate orientation of the waveguide.

There are four transitions which provide a direct measurement of $\$$: αe, αf, βe, and βf. The first was chosen because it is relatively isolated if the microwave field is parallel to the magnetic field. The second was rejected because the cyclotron resonance is nearby and of the same polarity. Both of the β transitions were rejected because of the closeness of the βe and βf crossings. Near these crossings any static electric fields which were present would quench the population of β states.

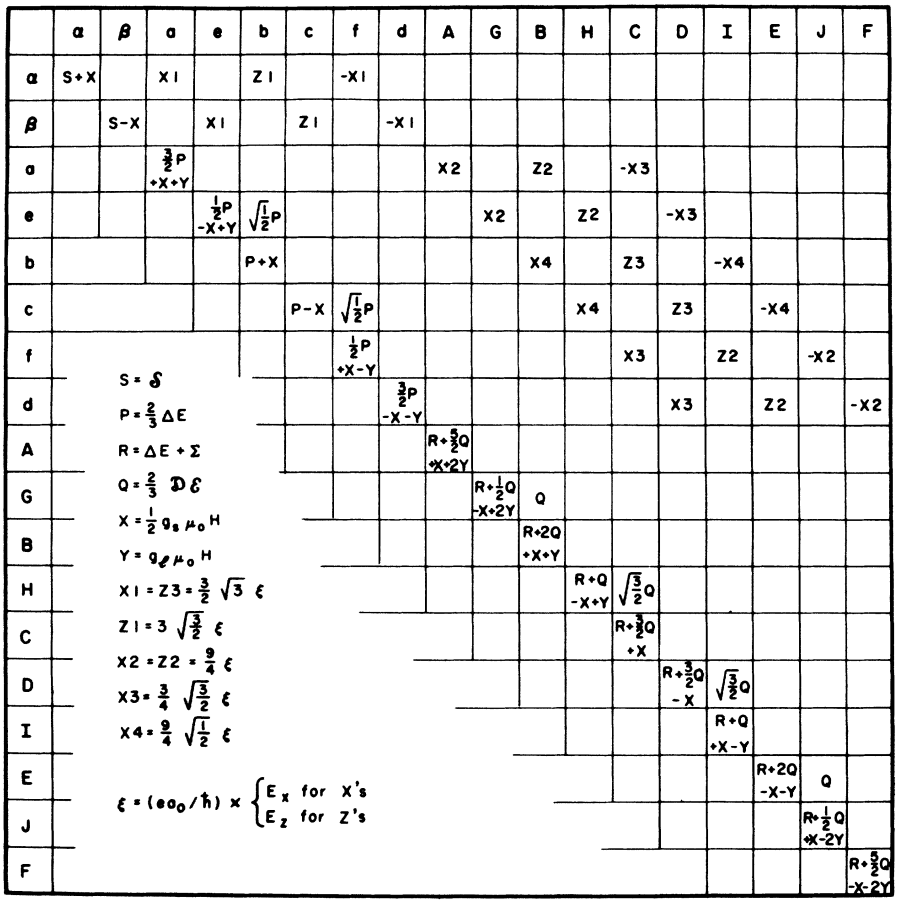

FIG. 2. Hamiltonian with Stark energy in the high-field representation. Only the upper half is shown. Stark shifts were calculated with appropriate values for the electric fields E_x and E_z. Microwave-induced transitions can be read off this figure, considering spin-orbit mixing, since the Stark elements contain electric dipole matrix elements.

The choice of αc and βd for the high-frequency measurement was determined mainly by available microwave equipment at 40 GHz. Unfortunately the βd resonance was studied near the βf crossing. However, αc and βd were well isolated from other microwave transitions in $n=3$ and in higher excited states of the ion.

D. Signal Due to Microwave-Induced Transitions

We consider two decaying states a and b coupled by a microwave field $\vec{E}$ of frequency ν. Helium ions are produced in these excited states at rates r_a and r_b by electron bombardment of helium gas. Optical decay of the states occurs with decay constants γ_a and γ_b. Spontaneous decay constants for $3S$, $3P$, and $3D$ states are 16.1, 483.3, and 164.7 MHz, respectively. A further contribution to the γ's can arise from collisions of the excited ions with ground-state atoms and ions. A theory of such collisions is presented in the Appendix.

Rate equations can be written for the numbers n_a and n_b of atoms in the excited states:

$$\dot{n}_a = r_a - \gamma_a n_a + W(n_b - n_a),$$
$$\dot{n}_b = r_b - \gamma_b n_b + W(n_a - n_b), \tag{2}$$

where the rate of induced transitions[10] is

$$W = \tfrac{1}{4}(\gamma_a + \gamma_b)V^2/[(\omega - \nu)^2 + \tfrac{1}{4}(\gamma_a + \gamma_b)^2]. \tag{3}$$

Here $\omega > 0$ is the transition frequency, and $V = e\vec{\chi}_{ab} \cdot \vec{E}/\hbar$ is the interaction matrix element in appropriate units. The electric dipole matrix element between the states is $e\vec{\chi}_{ab}$.

In the steady state $\dot{n}_a = \dot{n}_b = 0$ and the populations of excited atoms, n_a and n_b, can be found. Since the excited states can decay to various lower levels, they do not all produce light to which the detector is sensitive. Let f_a and f_b be the fractions of these decays which lead to light of the wavelength detected. Since we detect $n=3$ to $n=2$ radiation (1640 Å) but not that from $n=3$ to $n=1$, the branching ratios are $f_S = f_D = 1$ and $f_P = 0.11$. The rate of emission of 1640-Å photons is

$$r(W) = f_a \gamma_a n_a + f_b \gamma_b n_b. \tag{4}$$

The microwave-induced signal found in a "lock-in" detection scheme is the change in $r(W)$ produced by symmetric square-wave modulation of the microwave field strength. With 100% modulation the signal is

TABLE II. The $n=3$ states in the high-magnetic-field limit. States of the same m are mixed by spin-orbit coupling. There are 28 σ-polarized ($\Delta m_l = \pm 1$) and 16 π-polarized ($\Delta m_l = 0$) electric dipole transitions at intermediate magnetic fields.

Name	l	m_l	m_s	m
α	0	0	$+\frac{1}{2}$	$+\frac{1}{2}$
β	0	0	$-$	$-\frac{1}{2}$
a	1	1	$+$	$+\frac{3}{2}$
e	1	1	$-$	$+\frac{1}{2}$
b	1	0	$+$	$+\frac{1}{2}$
c	1	0	$-$	$-\frac{1}{2}$
f	1	-1	$+$	$-\frac{1}{2}$
d	1	-1	$-$	$-\frac{3}{2}$
A	2	2	$+$	$+\frac{5}{2}$
G	2	2	$-$	$+\frac{3}{2}$
B	2	1	$+$	$+\frac{3}{2}$
H	2	1	$-$	$+\frac{1}{2}$
C	2	0	$+$	$+\frac{1}{2}$
D	2	0	$-$	$-\frac{1}{2}$
I	2	-1	$+$	$-\frac{1}{2}$
E	2	-1	$-$	$-\frac{3}{2}$
J	2	-2	$+$	$-\frac{3}{2}$
F	2	-2	$-$	$-\frac{5}{2}$

$$S_{ab} = r(W) - r(0) = A V^2/(F + GV^2), \tag{5}$$

where the amplitude is

$$A = -\tfrac{1}{4}(f_a - f_b)[(r_a/\gamma_a) - (r_b/\gamma_b)](\gamma_a + \gamma_b)$$

and

$$F = (\omega + \Delta - \nu)^2 + \tfrac{1}{4}(\gamma_a + \gamma_b)^2,$$

$$G = \tfrac{1}{4}(\gamma_a + \gamma_b)^2/(\gamma_a\gamma_b).$$

Since F appears in the denominator of S_{ab} and is quadratic in ω, the signal is a Lorentzian in ω centered at $\omega + \Delta = \nu$. Writing $\omega = \omega_0 + g(H)$, where ω_0 is the theoretical fine-structure separation at zero magnetic field, we see that the signal would be Lorentzian in H if g were linear and V were field independent. It can also be seen that Δ is the experimental correction to ω_0 found by fitting the Lorentzian to a measured resonance curve.

Since V is proportional to the microwave electric field E, we have V^2 proportional to the microwave power M. The signal is linear in power at low power, departs from linearity due to the term GV^2 in the denominator, and approaches an asymptote at high power as the transition becomes saturated. The condition for 50% saturation at resonance and 41% increase in the width at half-height is $V^2 = \gamma_a\gamma_b$.

In general, the nonlinearity with power of the signal due to a transition depends on how far from resonance it is, as well as on its γ's and matrix element. If the observed signal contains contributions from transitions other than those included in the expression with which data are fitted, an erroneous value for Δ will be obtained. Since the position and size of the interloping resonances relative to the main resonance depend on microwave frequency and power, so will the value of Δ. Thus, since different transitions have a different Zeeman effect and approach saturation at different power levels, a search for power and frequency effects on Δ is a test for the importance of unknown transitions. A further test for narrow, nearby resonances is to measure signals at different places on the main resonance curve.

E. Normalizing Signal and Angular Distribution of Light

The amplitude A for the lock-in signal expression given above contains the rates of excitation. These rates are proportional to the bombarding electron current. Since the electron optics depends on the magnetic field, so will the rates of excitation. Thus the amplitude A was field dependent, and resonance curves were slightly distorted. To remove this distortion, lock-in signals were divided by a normalizing signal, chosen as the total light signal in the absence of microwave power. A possible error in the use of the total light for normalization is discussed in Sec. IV A.

The 1640-Å light from a specific $n=3$ P or D state has an angular distribution. The total light

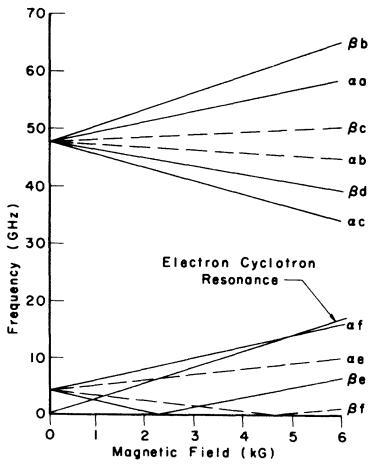

FIG. 3. Frequencies of S-to-P transitions. Solid lines are σ- and dashed lines are π-polarized transitions. With a microwave frequency of 40 GHz, αc was centered at 3.5 kG and βd at 5.7 kG. Low-frequency transition αe was studied at fields from 4 to 5 kG. The βe crossing at 2.3 kG gave the ion velocity. The βf crossing at 4.7 kG caused unfortunate shifts of βd.

used for normalization, however, can be shown to be isotropic if the rate of excitation does not depend on m_l or m_s. This is expected to be the case. Since the detector observes light predominantly in a direction perpendicular to the magnetic field the angular distribution is of interest in a consideration of a microwave-induced signal involving two states. There are two effects. First, the amplitude A will contain different f's from those given in Sec. II D. For example, the term $(f_a - f_b)$ for the βd transition is 8% larger than for αc if light is observed perpendicular to the magnetic field, whereas this term would be equal with an omnidirectional detector. The second effect is a slight magnetic field dependence in the angular distribution of light from P and D sublevels which have $|m_l| < l$. This results in a field-dependent amplitude for the αc and αe resonances. Fortunately the resulting distortion causes negligible shifts of the resonances.

III. APPARATUS

A. Magnet and Magnetic Field Measurement

The magnetic field was provided by an iron-core magnet (Varian V-3603), indicated in Fig. 4, with 30-cm pole pieces separated by 9.5 cm. The power supply (Varian V-FR2503) was regulated by a Hall-effect probe which ensured field stability better than 0.05 G/h. Gradients in the field at the site of the interaction region were less than 0.05 G/cm. Since the slope of a microwave transition frequency is the order of 1 MHz/G no corrections were made for field stability or homogeneity.

A Magnion G-502 NMR spectrometer, modified to permit low modulation amplitude, was used for field measurement. The probe used during data taking (the "working probe") was positioned 3.5 cm from the interaction region. Since this probe was close to a pole piece, there was some inhomogeneity in its vicinity resulting in a different NMR reading from that in the interaction region. In order to make a correction for the position of the probe, the vacuum chamber was opened periodically and a second probe was placed in the interaction space. Readings were taken with both probes at several magnetic field points spanning the range over which precision data were taken. The "NMR probe position correction" was the interaction-space reading minus the working-probe reading. This correction varied across a resonance and was as large as 0.5 G. Before analysis of precision data the appropriate position correction was added to the working-probe reading for each data point. These corrected NMR frequencies were then used to evaluate $\mu_B H$ for use in the Zeeman problem.

Since the probes contained water, the NMR frequency was

$$\omega_{\mathrm{NMR}} = \mu_B g_W H/\hbar ,$$

where g_W is the effective proton g value in water. The ratio g_J/g_W, where g_J is the g value of the hydrogen ground state, has been measured accurately.[17] Converting g_J to g_s with a theoretical multiplicative factor of $\eta = (1 - \frac{1}{3}\alpha^2)^{-1}$, we write

$$g_s \mu_B H/\hbar = \omega_{\mathrm{NMR}}\, \eta g_J/g_W. \tag{6}$$

Finally, the magnetic interaction of Eq. (1) is

$$\mathcal{H} = \eta g_J/g_W [m_s + (g_l/g_s) m_l]\omega_{\mathrm{NMR}} . \tag{6'}$$

B. Gas System

1. *Gas Supply*

A continuous-flow gas system was used to ensure

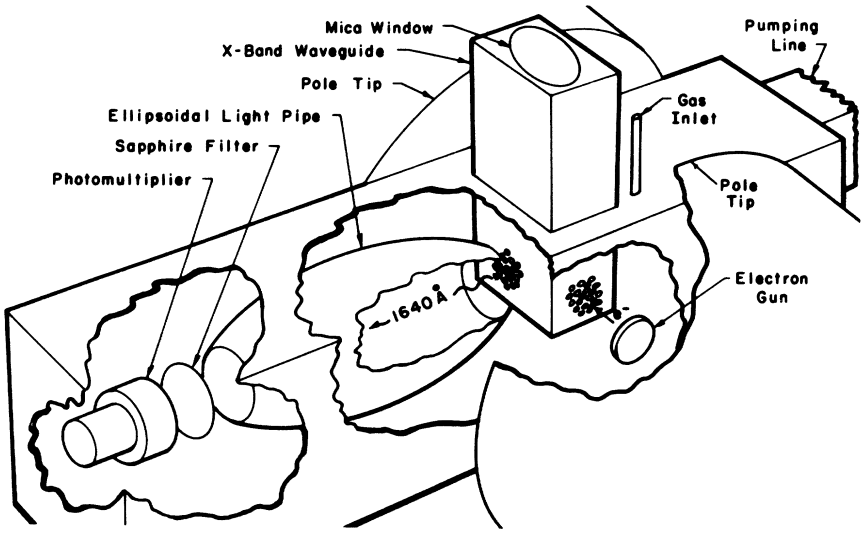

FIG. 4. Vacuum envelope and magnet. Waveguide is shown oriented for αc and βd.

the purity of the gas under observation. Helium (He^4) was admitted into the vacuum envelope through a 0.01-cm-bore metal capillary immersed in oil for temperature stability. The length of the capillary was chosen so that a satisfactory range of operating pressures could be obtained through adjustment of the two-stage metal-diaphragm pressure regulator on the supply tank.

Operating pressures were measured with a Pirani gauge (CVC GP-210) and an ion gauge (Heraeus IONIVAC 2), with helium calibration factors of 1.0 and 5.5, respectively. Pressure measurements given in the following sections were Pirani-gauge readings and are 30% lower than ion-gauge readings.

2. *Vacuum System*

The vacuum pumping station (Welch 3102A) had a 260-liter/sec "oil-free" turbomolecular pump chosen because of the high gas flow at relatively high pressures. The experimental region and optical system were contained in a vacuum envelope fabricated from stainless steel and aluminum. The ultimate vacuum obtainable in this system was 1.0×10^{-6} Torr. Analysis of the residual gas with a partial-pressure gauge (Varian 974-0036) showed mainly air and water vapor.

C. Basic Experimental Region

1. *Waveguide Structure*

The waveguide structure consisted of a vertical section of X-band copper waveguide passing through a mounting flange which was sealed to the vacuum chamber. The vacuum envelope was completed by a mica waveguide window at the top of the structure. The waveguide was shorted below the interaction region, which was situated in the center of the magnet gap. Sets of holes drilled in a honeycomb pattern in the walls of the waveguide faced the electron bombarder and photomultiplier, respectively. A further set of holes in the wall opposite the bombarder permitted most of the bombarding current to reach a collector.

2. *Electron Bombarder*

The electron bombarder, mounted on the waveguide structure, had supporting members of tantalum sheet and alumina rods. A large-area cathode was desired to minimize electric fields in the electron beam, leading to the choice of an indirectly heated 1-cm-diam Philips's type A cathode. The magnetic effects of heater current were minimized by the use of a noninductively wound heater carrying 21-kHz current. The collector current was regulated by a servoloop which controlled the voltage applied to the heater.

D. Optical System

A photomultiplier faced the interaction region along a horizontal axis perpendicular to the magnetic field. In order to reduce the effect of the magnet's fringing field on its operation, the photomultiplier was placed in a double magnetic shield 71 cm from the center of the magnet. Optical coupling was increased by an ellipsoidal mirror.

The signal to be detected was the 1640-Å light from the $n = 3$ to $n = 2$ decay of He^+. The 18-stage end-on photomultiplier (EMR 542G-08-18) with a semitransparent cesium iodide photocathode and lithium fluoride window had, at 1640 Å, a 4% quantum efficiency which decreased to 0.004% at 2500 Å. Since the window transmitted to 1050 Å, a sapphire filter with a cutoff about 1400 Å was used to block the 1215-Å light from the $n = 4$ to $n = 2$ decay of He^+, and the L_α light from any atomic hydrogen that may have been present.

E. Microwave System

1. *High Frequency*

A two-cavity klystron oscillator (Varian VA-534) phase-locked at 39 820.00 MHz provided 1.5 W of microwave power. The reference frequency applied to a crystal mixer for phase-locking was supplied by a sweep oscillator (HP H01-694A) phase-locked at 9970.00 MHz. The klystron frequency was then locked 60.000 MHz lower than the fourth harmonic of the reference frequency by an oscillator synchronizer (Micro-Now 202). Following two 20-dB isolators in tandem to prevent phase-lock disruptions during modulation, the desired power level was set on an attenuator. Modulation at 37 Hz was accomplished by a 20-dB ferrite switch that switched the power either to a dummy load or to the line leading to the experiment. In this line were a slide screw tuner and two 20-dB couplers for a crystal and a thermistor mount used in power measurements.

For power leveling, the crystal provided a voltage which was servo-leveled during the "on" portion of the modulation cycle. Saturation of the leveling amplifier during the "off" portion of the cycle was avoided by placing a diode in its feedback loop. Leveling and modulation were both obtained with the same ferrite switch through current summing of the leveling and modulating bias.

The microwave line described above consisted of R-band (26–40 GHz) components. A tapered section was used to join the R-band line to the X-band waveguide in the basic experimental region. The larger sized X-band waveguide was used in order to obtain a larger interaction region, approximately 1 cm^3.

2. *Low Frequency*

The output of a phase-locked isolated sweep os-

cillator (HP H01-694A) was square-wave modulated and leveled in an 80-dB *p-i-n* diode attenuator before amplification to the desired level in a traveling-wave-tube (TWT) amplifier. The microwave power then entered a line similar to that described above, with a tuner and couplers for a crystal and thermistor mount.

F. Measurement of Signals

In order to extract the microwave-induced signal from the total light, the microwave power was square-wave modulated and the photomultiplier output current was synchronously demodulated in a lock-in detector (PAR HR-8). Resonance curves so obtained were slightly distorted because of magnetic field dependence in the spreading of the bombarding electron beam. To deal with such distortions, lock-in signals were divided by the appropriate photomultiplier output currents. Two different microwave power levels were used at each magnetic field point. Lock-in signals and the photomultiplier current were measured with an integrating digital voltmeter (DY 2401C), and the NMR oscillator frequency was measured with a frequency counter (HP 5245L) whose internal frequency standard was periodically compared with WWV. A signal scanner (HP 2901A) was used to automatically program and record on perforated tape the following quantities at each magnetic field point: (i) NMR frequency using the working probe, (ii) lock-in baseline (microwave power turned off), (iii) high-power lock-in signal, (iv) photomultiplier output current (microwave power turned off), (v) low-power lock-in signal.

The time constant in the output amplifier of the lock-in detector was 100 msec. Following a 2-sec pause between readings, the lock-in signal was integrated for 100 sec and the photomultiplier current for 10 sec. After the above scan was taken at one field point, the next point was automatically set by means of a motor-driven potentiometer in the magnet's regulating system. The NMR oscillator was then tuned to the new point and another scan was begun.

IV. OBSERVATIONS

A. Operating Characteristics

1. *Size of Photomultiplier Current*

To estimate the size of the photomultiplier current we take the product of the following quantities: (i) photomultiplier gain $\approx 2\times10^6$ at 3100 V, (ii) quantum efficiency of 0.04 at 1640 Å, (iii) transmission of sapphire filter ≈ 0.7, (iv) fraction of the light entering the ellipsoid = 0.06, (v) efficiency of the ellipsoid ≈ 0.3, (vi) transmission of the honeycomb pattern of holes in the waveguide = 0.5, (vii) effective length of the electron beam = 1 cm, (viii) number of helium atoms per $\text{cm}^3 = 3.5\times10^{13}\,P$, where P is the pressure in mTorr, (ix) bombarding electron current $= 10^{-3}\,I$, where I is in mA, (x) cross section for producing 1640-Å light.

We use the "sudden approximation" of Lamb and Skinner[4] to estimate the cross section for the S state. One contribution to the cross section is the ionization cross section ($0.27\pi a_0^2$ for 400-V bombarding electrons) times the squared overlap integral (0.0017) between the $3S$ state and the ground state for one electron, with $Z = 1.69$.

An additional mechanism for exciting S states and the only way, within the framework of the sudden approximation, for exciting P and D states is atomic excitation $\sigma(1S, 3l)$ in which one electron is raised suddenly to $3l$, followed by ionization (probability = 1.1%) of the remaining electron because of the sudden change in its effective nuclear charge. According to Massey,[18] the appropriate cross sections for atomic S, P, and D states are $7\times10^{-4}\pi a_0^2$, $1.3\times10^{-2}\pi a_0^2$, and $1.5\times10^{-4}\pi a_0^2$ for 400-V electrons. Taking an ionic P-state branching ratio of 11%, we find a cross section of $4.9\times10^{-4}\pi a_0^2$ for producing 1640-Å light. Then, with a current of 4 mA and pressure of 10 mTorr the estimated photomultiplier current is 3.4×10^{-5} A. The observed current under these conditions was 3×10^{-6} A, a factor of 11 smaller. Although this factor is within the uncertainty of the estimate, there is an indication that the cross section has been overestimated by the sudden approximation, perhaps because the first electron changes its state more slowly than demanded by the sudden approximation. In the limit where the first electron changes its state very slowly, the cross section would be zero. Thus it appears that the actual cross section falls between the limits predicted by "suddenness" and "slowness."

2. *Noise*

Using the above value of gain and the observed photomultiplier current we find a photocathode current of 1.0×10^7 electrons/sec. The fractional deviation in successive 20-sec periods is expected to be 0.007%, in good agreement with the observed noise of 0.005%.

3. *Size of Saturated Signal*

As the microwave power was increased, the lock-in signal due to a single resonance approached a value of 18% quenching. Dividing the atomic S, P, and D cross sections given above by $2(2l+1)$, we obtain rates for use in a signal expression of the type shown in Sec. II D, leading to an expected saturated signal of 41% quenching. Agreement with the observed value of 18% could be obtained through decreasing σ_S relative to σ_P and σ_D since the sudden approximation yields $\sigma_S/\sigma_P = 3.3$ and

$\sigma_S/\sigma_D = 285$. If instead of the sudden approximation we assume equipartition, we would have $\sigma_l \propto (2l+1)$. Equipartition could arise if the ionized electron left the atom so slowly that its field thoroughly mixed the various sublevels of the remaining electron. With equipartition, the saturated signal would be 7%. Thus we again find an observed operating characteristic falling between the sudden limit and the slow limit.

4. *Excitation Curves*

The excitation curves shown in Fig. 5 have a threshold for $n = 3$ excitation of the ion at about 75 V, close to the expected threshold of 72 V. The total light signal has a plateau down to 20 V, the threshold for excitation of the helium atom. The plateau may be due to fluorescence of the sapphire window upon absorption of ultraviolet light from the atom. There is a slight lock-in signal below the $n = 3$ threshold which is too small to have a significant effect on the fine-structure measurements. Above the $n = 3$ threshold the curves rise rapidly up to 200 V, where some data were taken. Most data were taken at 400 V, where the lock-in signal has a maximum.

5. *Total Light Signal*

Figure 6 shows the total light signal over a wide range of magnetic field with no microwave power present. The general decrease with magnetic field indicates a field dependence in the electron optics of the bombarding beam, mentioned in Sec. II E. An additional feature is the presence of the βe crossing notch at 2.3 kG, which fortunately does not cause significant shifts of the lock-in resonance

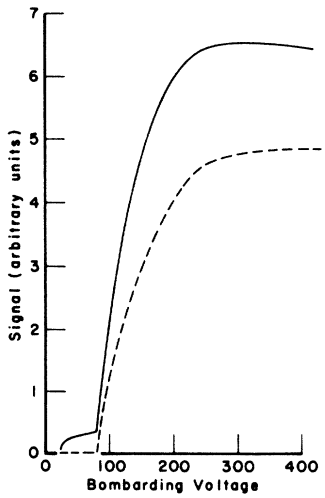

FIG. 5. Excitation curves normalized to unit bombarding current. Lock-in signal (dashed line) nearly vanishes below the threshold at 75 V, but the photomultiplier current has a small plateau down to 20 V.

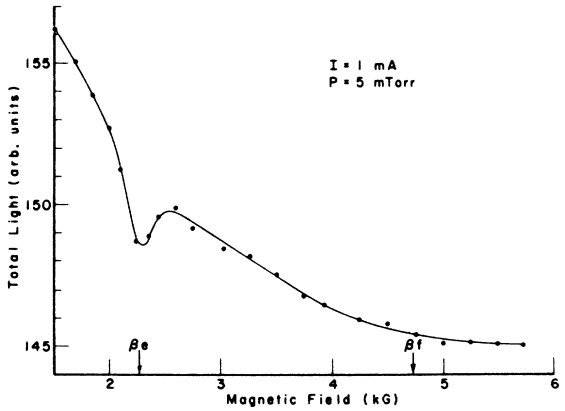

FIG. 6. Total light panoramic. Solid curve is a fitting function with a power series in H for the gross structure and appropriate Lorentzians for βe and βf.

curves when the total light is used for normalization. The size of the βe and βf crossing notches can be used as a measure of the electric fields present in the interaction region. The βe notch is always present because of the motional electric field $\vec{v}\times\vec{B}$. Depending on their direction, additional electric fields may increase the size of βe, or make βf show up. The curve shown in Fig. 6 was taken at low pressure and low bombarding current. Since βf hardly appears we may assume that the βe notch is due mostly to the $\vec{v}\times\vec{B}$ field. The size of the notch corresponds to an ion velocity of 1.3×10^5 cm/sec, in agreement with the expected[5] thermal velocity.

B. Panoramics of Lock-in Signal

The lock-in signal was observed over a wide range of the magnetic field at several microwave frequencies and power levels in a search for resonances. It was expected that transitions in levels with $n > 3$ would be observed because atoms in these levels can decay to $n = 3$ and then to $n = 2$, producing 1640-Å light. Such transitions were expected at low microwave frequencies, since fine-structure intervals scale as n^{-3}. For example, the large interval ΔE in $n = 7$ is about equal to s in $n = 3$.

1. *High Frequency*

Figure 7 shows the normalized signals (lock-in divided by total light) found with transverse microwave polarization at 40 GHz. All of these signal points were included in a fit to a signal expression taken as the sum of Lorentzians (see Sec. II D) for the αc and βd transitions. The parameters were the microwave field and an amplitude for each resonance, $A_{\alpha c}$ and $A_{\beta d}$. These amplitudes were expected to be equal except for a possible effect

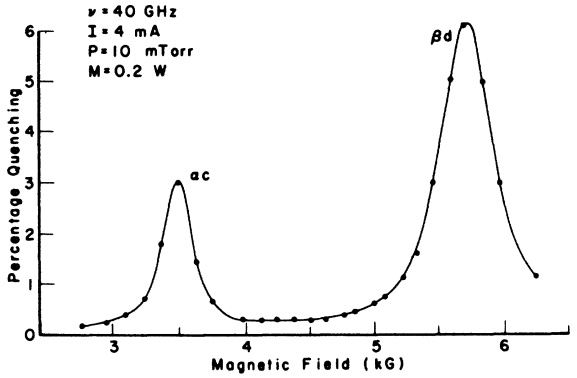

FIG. 7. High-frequency panoramic. All the points are fitted with a sum of Lorentzians for αc and βd. rms difference between theory and experiment is 0.02 percentage quenching and there appear to be no unexpected resonances.

up to 8% discussed in Sec. II E because of the different angular distribution of light from the c and d states. The fitted relative amplitude $R = A_{\beta d}/A_{\alpha c}$ was 1.07. Although this result indicates an angular distribution effect, the value of R used in Sec. IV F for making overlap corrections was taken as 1.0 ± 0.1. The fit of the theoretical curve to the data was sufficiently close so that no interloping resonances could be seen in a plot of the difference between experiment and theory. None were expected, since transitions in $n > 3$ lie below 40 GHz in this range of magnetic field.

2. *Low Frequency*

Figure 8 shows the normalized signal obtained at 9 GHz with the "parallel" waveguide orientation, at a moderate power level of 0.27 W, which is close to producing 50% saturation of the $n = 3$ αe transition. The solid curve is a Lorentzian fitted to points on the main resonance. The low point at 3.1 kG is on the cyclotron resonance which was excited by a small transverse component of the microwave field. The slight rise near 2.5 kG is the $n = 3$ αf resonance driven by the same component. At 7 kG, we see the $n = 4$ αe resonance and infer from its height that $4S$ states are excited at a rate 0.6 times that of $3S$ states.

Since the decay rates (γ's) vary roughly (for $n > 2$) as n^{-3}, and matrix elements for $S \rightarrow P$ transitions as n^2, the saturation criterion given in Sec. II D indicates that the microwave power to obtain 50% saturation of an $S \rightarrow P$ transition varies as n^{-10}. Thus a high n transition will still be saturated at an extremely low power level where most of the $n = 3$ signal has disappeared. In Fig. 9, we show a panoramic taken at 9 GHz with a power of 0.0005 W. Each point represents one hour of signal integration. The solid curve contains Lorentzians

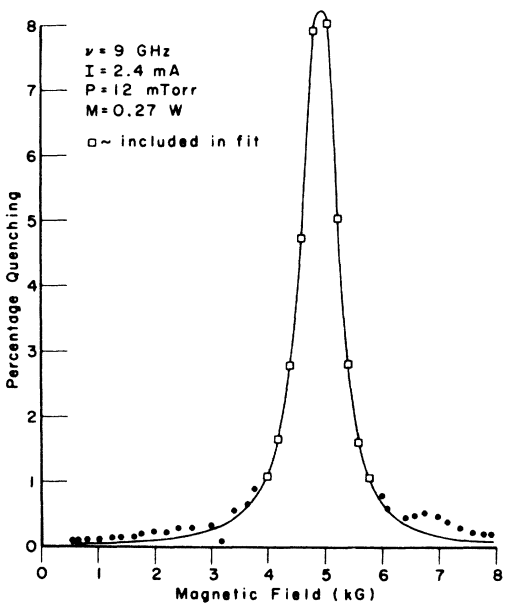

FIG. 8. Low-frequency panoramic. Curve is a Lorentzian for αe fitted to the 10 points with quenching over 1%. The cyclotron resonance at 3.1 kG and αf at 2.5 kG result from an unwanted transverse component of the microwave field. At 7 kG, the $n = 4$ αe resonance is seen because of the cascade process.

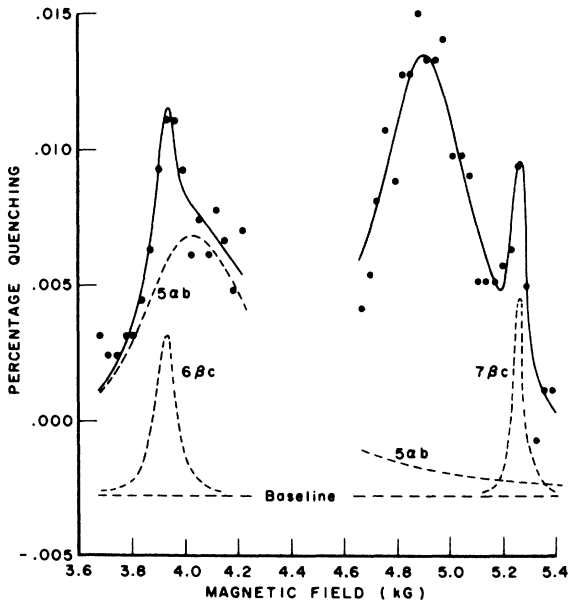

FIG. 9. Very low-power panoramic taken at 9 GHz with 0.0005 W. Each point represents 1 h of signal averaging. Solid curve is a theoretical fit. Main resonance is $3\alpha e$ centered at 4.9 kG with a height about $\frac{1}{1000}$ of its saturated height. Other resonances are shown as dashed lines with their bases on the fitted base line of -0.0035 percentage quenching.

for $3\alpha e$, $5\alpha b$, $6\beta c$, $7\beta c$, and an additive constant (a base line). The microwave field was inferred from the power measurement and comparison with the value of E^2 found at moderate power. Supposing that the detector is sensitive only to 1640 Å, we calculated effective branching ratios considering all the possible decay paths. The amplitudes for $S \rightarrow P$ transitions depend mainly on the rate of exciting S states, rather than P states, because $\gamma_S \approx 0.03\gamma_P$ (for $n > 2$). The parameters varied by the fitting routine were the base line and rates of excitation for S states in $n = 3$, 5, 6, and 7. The fitted rates relative to $n = 3$ were 0.83, 0.50, and 0.73 for $n = 5$, 6, and 7, respectively. These are considerably higher than expected from an n^{-3} variation. This could be due to the detection of light other than 1640 Å. In any case, the observed amplitude of these resonances can be used to evaluate their effect on fine-structure determinations. Additional low-power panoramics were taken at 8 and 10 GHz and $S \rightarrow P$ transitions in $n = 5$ to 9 were found. Their amplitudes were determined with a consistency of about 30%.

C. Shifts Due to Interloping Resonances

The major problem with a direct measurement of δ was shifts due to the presence of resonances other than $3\alpha e$. The importance of these interloping resonances was discovered through the dependence of measured fine structure on microwave power. The most dramatic example of a power shift is given in Fig. 10, where a 4-MHz drop occurs when the power is reduced an order of magnitude from the 50% saturation level. This drop

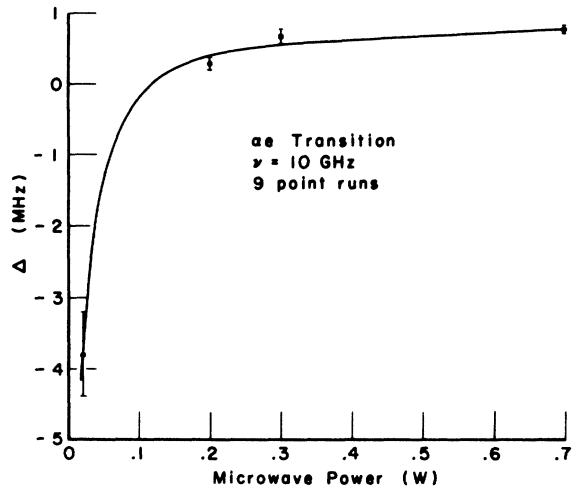

FIG. 10. Power shift of $\Delta\delta$. The power dependence of the raw Δ's is fitted with the extrapolation formula. Large shift at low power is due to the $7\beta c$ resonance. In this case, set 12, the extrapolated value of Δ is 0.8 MHz (see text).

can be attributed entirely to $7\beta c$. We included $7\beta c$ in the line-shape expression with an amplitude 20% greater than its average found in the low-power panoramics. When the data leading to Fig. 10 were reanalyzed, the fine-structure corrections became 0.84 ± 0.58, 0.90 ± 0.07, 1.10 ± 0.09, and 1.03 ± 0.04 MHz at power levels of 0.02, 0.2, 0.3, and 0.7 W, respectively. We see that the inclusion of $7\beta c$ in the analysis has removed the power effect at 10 GHz. The reason for the strong power effect was the accidental location of $7\beta c$ near the high-field half-height point of $3\alpha e$. The shifts due to $7\beta c$ are the difference between the values of δ found without, and with, $7\beta c$ included in the analysis. These shifts are -4.64, -0.59, -0.44, and -0.26 MHz at the power levels of 0.02, 0.2, 0.3, and 0.7 W, respectively. These shifts come within 0.1 MHz of being given by an M^{-1} rule, where M is microwave power. This surprising power dependence can be seen in terms of a simple model.

Suppose signals are measured at the center and the two half-height points of an unsaturated resonance, and that a small interloper is centered at one of the half-height points. If the interloper is sufficiently narrow, it can be shown that the power shift of the composite resonance is proportional to the height of the interloper relative to the main resonance, i.e., $\Delta \propto (M + M_s)^{-1}$, where M_s is the power for 50% saturation of the interloper.

According to the criterion given in Sec. IID, the $7\beta c$ transition requires $\frac{1}{500}$ as much power for 50% saturation at its center as does $3\alpha e$ (considering matrix elements at the relevant magnetic fields). At the lowest power in Fig. 9, therefore, $7\beta c$ is highly saturated even though $3\alpha e$ is nearly unsaturated. Thus, in this range of power, we may neglect M_s in the above formula leading to a shift of the observed resonance curve nearly proportional to the reciprocal of the power.

Calculations were also made of the shift expected from the 43 other $n = 3$ resonances and from the 102 $n = 4$ resonances. The resultant curve of shift vs power was nearly linear and had an intercept at zero power less than 0.2 MHz for frequencies of 8, 9, and 10 GHz.

For the two cases that have been discussed above, power shifts are given to within 0.2 MHz by either an M^{-1} or M dependence on power. Even if many different resonances contribute to the shifts, there is some reason to suppose that a linear combination of the M^{-1} and M terms will come within 0.5 MHz of describing them. In addition, a linear term would exactly describe the "rf Stark shift"[19] equal to $V^2/4\nu$, where V and ν are defined in Sec. IID. In the present paper, we shall therefore fit the observed power dependence of fine-structure measurements with these two terms in M.

D. Fine-Structure Determinations

1. *Extraction of Raw Δ's*

The procedure for taking data in high-precision runs is given in Sec. III F. The normalized signals so obtained were "least-squares" fitted through variation of parameters by an iterative fitting program that solves the "normal" equations. Lorentzian signal expressions of the type given in Sec. II D were used and the parameters in Eq. (5) that were varied were the amplitude A, microwave field strength E^2, and fine-structure correction Δ. The low-frequency data were analyzed with a Lorentzian for αe. High-frequency analysis used a sum of Lorentzians for αc and βd with common parameters.

2. *Search for Systematic Effects*

The dependence of Δ on experimental conditions was investigated for each of the transitions in a search for systematic effects. Several values of microwave power, helium pressure, and bombarding current were used. The number of magnetic field points N_H at which signals were measured was 3, 5, or 9. The bombarding voltage was lowered from 400 to 200 V for a few runs on αe and βd. In a test of the need for the sapphire filter, it was removed for a few runs on αc. Data were taken on αe at several microwave frequencies.

3. *Extrapolation*

The physical parameters that had an appreciable effect on the raw Δ's were the power, pressure, and current. A theory of these dependences is required in order to extract a final value from the raw measurements. For shifts with pressure P and current I, it is believed (see Appendix) that a linear extrapolation to zero P and PI is sufficient. For power shifts due to other resonances and the rf Stark shift a procedure has been described in Sec. IV C. A term linear in power M and a term in M^{-1} should be a reasonable approximation to such shifts. Combining terms for all these shifts, we write an extrapolation formula with which the observed fine-structure determinations were fitted,

$$\Delta_{fit} = \Delta_0 + C_{-1} M^{-1} + C_1 M + C_P P + C_{PI} PI \quad . \qquad (7)$$

Here Δ_0 is the value of Δ one would obtain in the absence of M, P, and PI shifts. Since the above terms are an approximate description of these shifts, Δ_0 is not an exact correction to the theoretical fine-structure value. However, it is felt that Δ_0 comes within 0.5 MHz of yielding the desired fine-structure intervals.

4. *Regression Analysis*

The raw Δ's were fitted with Eq. (7) by a regression analysis program[20] that provides a coefficient and its standard deviation for each independent variable. Observations were weighted according

TABLE III. Extrapolation of Δ the fine-structure correction for various sets of data, some of which are given in subsequent tables. The correction to S is obtained from the αe transition, and αc and βd yield a correction to $\Delta E - S$. The extrapolated value is Δ_0 and the C's are coefficients in Eq. (7) [Eq. (8) for βd]. Coefficients are missing when there were insufficient data to find them. In sets 8, 10, and 12, signals were measured at nine points on the resonance curve, whereas in the remainder of the αe sets (except set 1), signals were measured at three points. The first five αe sets were not included in the final result for reasons given in the references.

Set No.	Transition	Frequency (GHz)	Δ_0 (MHz)	C_{-1} (MHz W)	C_1 (MHz/W)	C_P (MHz/mTorr)	C_{PI} (MHz/mTorr/mA)
1[a]	αe	9	−0.02 ± 0.50	• • •	• • •	−0.05 ± 0.04	0.007 ± 0.003
2[b]	αe	10	−0.63 ± 0.69	−0.10 ± 0.22	0.2 ± 0.3	0.00 ± 0.01	−0.004 ± 0.002
3[b]	αe	9	0.76 ± 0.18	−0.13 ± 0.04	• • •	−0.01 ± 0.02	0.001 ± 0.003
4[c]	αe	8	−0.15 ± 0.22	−0.03 ± 0.01	0.5 ± 0.1	−0.04 ± 0.02	• • •
5[d]	αe	9.5	0.72 ± 0.76	−0.10 ± 0.12	• • •	• • •	0.010 ± 0.011
6	αe	9.5	0.57 ± 0.22	−0.17 ± 0.05	−0.1 ± 0.4	• • •	• • •
7	αe	8.5	0.27 ± 0.65	−0.09 ± 0.08	0.3 ± 0.9	• • •	• • •
8	αe	8	0.41 ± 0.05	−0.03 ± 0.01	• • •	• • •	• • •
9	αe	9	0.74 ± 0.25	−0.12 ± 0.03	0.0 ± 0.4	• • •	• • •
10	αe	9	0.87 ± 0.25	−0.04 ± 0.03	• • •	• • •	• • •
11	αe	10	0.56 ± 0.11	• • •	• • •	• • •	• • •
12	αe	10	0.82 ± 0.20	−0.10 ± 0.02	0.1 ± 0.3	• • •	• • •
13	αc	40	−0.31 ± 0.31	−0.00 ± 0.01	1.0 ± 0.3	0.05 ± 0.04	0.001 ± 0.004
14	βd	40	0.77 ± 0.18	• • •	0.5 ± 0.3	0.10 ± 0.02	0.089 ± 0.013

[a]Data taken with a preliminary form of the apparatus.
[b]Electron gun developed white flakes.
[c]Disagrees with 9-point runs taken at the same frequency, set 8.
[d]Bombarding voltage was 200 V, rather than the usual 400 V.

to $1/\sigma^2$, where σ is the deviation of the mean for the runs comprising the observation. In cases where σ was less than 0.1 MHz, the weight was set at 100.

5. *Some Small Corrections*

A correction for the quadratic Zeeman effect[14] raises the αc and lowers the βd result by 0.03 MHz The αe result is raised 0.02 MHz. The correction for the motional Stark shift due to the velocity given in Sec. IV A is +0.02 MHz for αc, −0.05 MHz for βd, and +0.11 MHz for αe.

E. Measurements on αe

The regression analyses for 12 sets of observations on αe are given in Table III, and the observations of certain sets are given in Table IV. Set 1 consists of 30 runs taken with an early form of the apparatus employing a cathode made of tungsten wire wound in a flat spiral. The photomultiplier was not shielded, the p-i-n diode modulator was a 40-dB type, and the magnetic field was scanned in only one direction. Cathode currents up to 16 mA at 200 V and pressures up to 90 mTorr were used. It is considered reassuring that these measurements are in essential agreement with later measurements at the same microwave frequency and power. Set 2 was the main basis for Ref. 8 and unfortunately is the most deviant of all the sets, differing from later measurements at the same frequency. This set and set 3 were both taken with the same cathode, which was covered with white flakes at the end of set 3. Possibly some of the white material was deposited in the interaction region and accumulated a charge, leading to a Stark shift independent of pressure and current. Set 4, consisting of 3-point runs, is thought to be of high quality, but its Δ_0 disagrees slightly with that of set 8, taken with 9-point runs at the same frequency. Set 5, like set 1, was taken at 200 V and agrees with other sets, indicating the absence of a voltage effect. Sets 6 to 12 are thought to be of high quality and form the basis of the s quotation.

Since some sets had only 3 or 4 observations, not all of the terms in Eq. (7) could be used. In six cases there were enough observations as a function of M to find C_{-1} and C_1. In one case, C_1 is significant and in 4 cases C_{-1} is significant. Therefore, in the remaining cases where there were at least four observations at different power levels, only the term in M^{-1} was used.

The P and PI terms are missing in those cases where P or I were not varied. The cases where P or I were varied are considered to provide information on the size of possible P or PI shifts in the remaining sets. For example, the average of C_P times the average pressure is −0.22 MHz. Treating this possible shift as an uncertainty rather than

TABLE IV. Observations on αe. N_H was the number of points taken on the resonance curve. P was the helium pressure, I the bombarding electron current, and ν the microwave frequency. Each run was taken with two microwave power levels M. The fine-structure correction found from fitting the observed resonance curve with a simple line shape is Δ_{raw}. In most cases, this agrees reasonably well with Δ_{fit}, a value obtained with the extrapolation formula, Eq. (7). The parentheses after certain run numbers indicate a number of runs that were grouped together.

						Low power			High power	
Set	Runs	N_H	P (mTorr)	I (mA)	ν (GHz)	M (W)	Δ_{raw} (MHz)	Δ_{fit} (MHz)	M (W)	Δ_{raw} (MHz)	Δ_{fit} (MHz)
4	445(13)	3	10	4	8	0.02	−1.73 ± 0.32	−2.17	0.05	−1.29 ± 0.12	−1.17
	431(7)	3	12	4	8	0.05	−1.19 ± 0.29	−1.24	0.25	−0.55 ± 0.09	−0.62
	438(11)	3	12	4	8	0.10	−0.73 ± 0.16	−0.89	0.70	−0.30 ± 0.04	−0.32
	400–11	3	10	4	8	0.14	−0.97 ± 0.12	−0.70	0.50	−0.49 ± 0.13	−0.36
	475–82	3	5	4	8	0.14	−0.44 ± 0.11	−0.51	0.50	0.25 ± 0.14	−0.17
	483(6)	3	2	4	8	0.14	−1.32 ± 0.32	−0.39	0.50	−0.29 ± 0.33	−0.05
	439(6)	3	12	4	8	0.90	0.06 ± 0.24	−0.21	2.0	0.51 ± 0.14	0.33
9	372–77	3	10	4	9	0.06	−0.89 ± 0.33	−1.20	0.25	0.32 ± 0.09	0.28
	362–71	3	10	4	9	0.12	−0.30 ± 0.09	−0.23	0.50	0.53 ± 0.08	0.52
	378–81	3	10	4	9	1.0	0.52 ± 0.31	0.65	•••	•••	•••
11	451–54	3	9	4	10	0.15	0.62 ± 0.25	0.56	0.30	0.75 ± 0.31	0.56
	447–50	3	9	4	10	0.50	0.36 ± 0.26	0.56	•••	•••	•••
8	787–89	9	10	2	8	0.03	−0.41 ± 0.14	−0.43	0.10	0.13 ± 0.05	0.16
	784–86	9	10	2	8	0.30	0.34 ± 0.02	0.33	0.70	0.12 ± 0.10	0.37
10	781–83	9	10	2	9	0.03	0.83 ± 0.42	−0.37	0.10	0.44 ± 0.05	0.50
	778–80	9	10	2	9	0.30	0.63 ± 0.11	0.75	0.70	1.08 ± 0.10	0.82
12	771–74	9	10	2	10	0.02	−3.80 ± 0.58	−3.91	0.20	0.31 ± 0.07	0.37
	775–77	9	10	2	10	0.30	0.66 ± 0.09	0.54	0.70	0.77 ± 0.04	0.77

a correction, we have a P-shift uncertainty of ± 0.11 MHz. In a similar fashion we find uncertainties of ± 0.07, ± 0.15, and ± 0.08 MHz for cases where a PI, M^{-1}, or M is missing in Table III. In addition, we add an uncertainty of ± 0.10 MHz for the NMR probe position correction to all the sets. The extrapolated Δ's and their total uncertainties for the 12 αe sets are shown in Fig. 11.

The final average of $\Delta_0 = 0.61$ MHz is based on the seven high-quality sets 6 to 12. Since the extrapolation formula may not remove all systematic effects, we do not take the standard deviation of the mean for the uncertainty quotation. Rather, we believe that the weighted average uncertainty, $\bar{\sigma} = 0.54$ MHz, represents a "68% confidence interval." We note that 75% of the 12 sets lie within $\bar{\sigma}$ of Δ_0 and 92% lie within $2\bar{\sigma}$. Furthermore, most of the raw Δ's fall in the range $\Delta_0 \pm \bar{\sigma}$ if we ignore low-power results. Adding the corrections given in Sec. IV D, we have the final result

$$\delta = 4183.17 \pm 0.54 \text{ MHz}$$

from measurements on αe.

F. Measurements on αc

We turn now to the measurement of the high-frequency interval $\Delta E - \delta$. A 40-GHz klystron was used for observations on αc and βd. The overlap problem encountered in the low-frequency work was not expected at 40 GHz because transitions in levels above $n = 3$ lie at lower frequencies and other $n = 3$ transitions are distant or of the other polarity and have frequencies nearly independent of magnetic field. (A magnetic-field-independent transition merely adds a constant base line to the signal.) The need to include the βd resonance in the signal expression when fitting αc runs was made obvious by a 1-MHz change in Δ between a 3- and 5-point run if βd was not included.

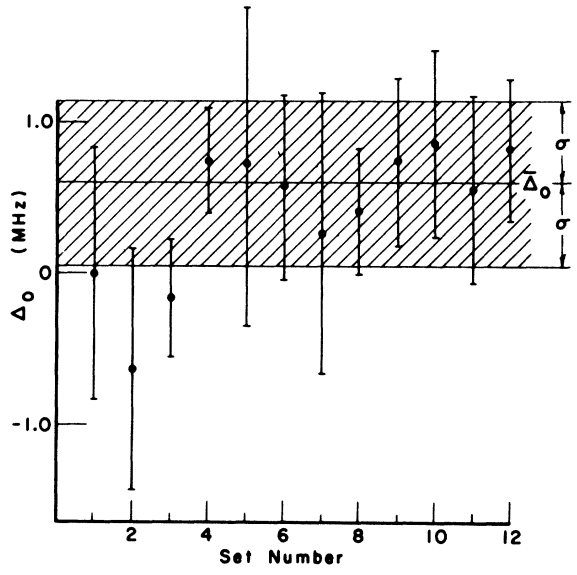

FIG. 11. Extrapolated Δ for αe. Twelve sets of observations are shown with their estimated total uncertainties. Last seven sets yield an average $\bar{\Delta}_0 = 0.61 \pm 0.54$ MHz.

Observations on αc (Table V) were fitted with Eq. (7). There is little evidence of a pressure and current effect since the P and PI coefficients shown in Table III differ from 0 by 1.4 and 0.2 standard deviations, respectively. However, the slope with microwave power is three standard deviations and is not understood, since it is about ten times larger than the "rf Stark" effect given in Sec. IV C. The M^{-1} term is not significant here. Runs 665–668, taken with no sapphire filter, have reasonable agreement with the values predicted by Eq. (7), indicating that there was no important light in the wavelength region between the LiF and sapphire cutoffs.

As mentioned in Sec. IV D, the raw Δ's were obtained with a line-shape expression in which the αc and βd resonances had the same amplitude factor A. We now inquire how a change in the relative amplitudes would affect the overlap correction. It is found that Δ's extracted from αc data differ by an amount

$$\delta_{\alpha c} = -(1.31 + 2.24M)A_{\beta d}/A_{\alpha c}$$

from Δ's found with βd absent from the line-shape expression. Since we extrapolate to zero M, and since we believe that $A_{\alpha c}$ and $A_{\beta d}$ differ by less than 10%, we expect an error in the overlap correction to αc of the order of ± 0.1 MHz. The overlap uncertainty and an uncertainty of 0.1 MHz for the NMR probe position correction are added to the standard deviation of Δ_0 found by the regression analysis. Adding the corrections given in Sec. IV D, we find

$$\Delta E - \delta = 47\,843.32 \pm 0.51 \text{ MHz}$$

from measurements on αc. This result is compromised by the existence of an unexpected and unexplained power effect.

G. Measurements on βd

Measurements of Δ obtained from βd had a considerable dependence on the power, pressure, and current. The pressure dependence was the most severe and is shown in Fig. 12. The power dependence is largely due to power broadening of the resonance in the presence of a given pressure and current asymmetry. This can be seen in a plot of Δ against pressure for the 1-mA data, where the low- and high-power curves have nearly the same intercept at zero pressure. Thus there is very little intrinsic power effect. The pressure and

TABLE V. Observations on αc. This table gives the data of set 13. See Table IV for an explanation of column headings.

					Low power			High power	
Runs	N_H	P (mTorr)	I (mA)	M (W)	Δ_{raw} (MHz)	Δ_{fit} (MHz)	M (W)	Δ_{raw} (MHz)	Δ_{fit} (MHz)
510–18	5	10	4	0.1	0.67 ± 0.08	0.32	0.2	0.56 ± 0.14	0.44
519–29	5	10	2	0.1	1.08 ± 0.19	0.31	0.2	0.63 ± 0.25	0.42
530–36	5	10	8	0.1	0.08 ± 0.19	0.34	0.2	0.32 ± 0.11	0.47
537–44	5	10	4	0.06	0.41 ± 0.44	0.26	0.3	0.29 ± 0.18	0.54
660–63	9	5	0.5	0.1	−0.29 ± 0.17	−0.03	0.8	0.92 ± 0.09	0.76
669–71	9	8	0.5	0.2	−0.06 ± 0.05	0.31	0.8	0.93 ± 0.14	0.92
672–75	9	2	0.5	0.2	0.39 ± 0.19	−0.02	0.8	0.66 ± 0.36	0.60
677–79	9	2	1	0.2	0.63 ± 0.33	−0.02	0.8	0.78 ± 0.18	0.60
680–81	9	5	1	0.2	0.01 ± 0.07	0.15	0.8	0.61 ± 0.05	0.76
665–68[a]	9	10	0.5	0.2	0.11 ± 0.05	0.39	0.8	0.85 ± 0.07	0.99
791–93	9	10	2	0.03	0.63 ± 0.28	0.16	0.08	0.21 ± 0.04	0.28
795–99	9	10	2	0.01	−1.06 ± 0.64	−0.09	0.02	−0.10 ± 0.31	0.09

[a]Not included in the regression analysis, since there was no sapphire filter.

current asymmetry are understood to be due to atom and ion quenching of the β state near the βf crossing which lies 1 kG lower than the center of βd. A theory of quenching is given in the Appendix and an expression for pressure and current shifts is found in terms of a coefficient U. This coefficient depends on the number N_H of field points at which signals are measured, and increases with microwave power. In analyzing βd observations (Table VI) we fit the raw Δ's with a modified form of Eq. (7)

$$\Delta_{fit} = \Delta_0 + C_1 M + U(C_P P + C_{PI} PI) \ , \qquad (8)$$

where the U's are given in Table VI. The resultant coefficients and their standard deviations are shown in Table III. The pressure and ion coefficients C_P and C_{PI} are 2.0 and 3.4 times, respectively, as large as estimated in the Appendix. These discrepancies could be the result of a calibration error in pressure measurements and an effective cathode emitting area smaller than expected, as well as a lack of validity of the calculation in the Appendix. In any case, the extrapolation of Δ to zero pressure and current is thought to be valid. The slope with microwave power can be explained by the "rf Stark shift" which has a slope of 0.2 MHz/W for βd and agrees within statistics with the observed slope of 0.5 ± 0.3 MHz/W.

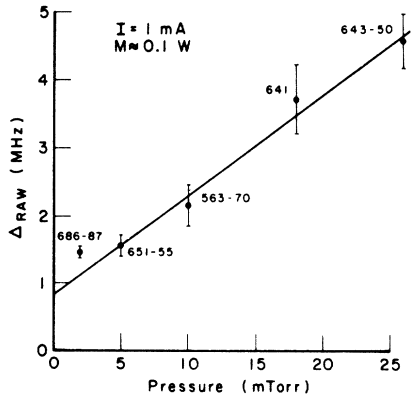

FIG. 12. Pressure shift of βd. Run numbers appear with each point. Line gives the shift for these points calculated by a regression analysis of all βd raw Δ's.

In a search for an effect with bombarding voltage, we see (Table VI) that at 200 V the two low-pressure results agree with the fitted Δ's, but the 19-mTorr result is an anomaly. Unfortunately, insufficient data were taken to make a separate extrapolation to zero P and I for 200 V. However, we assume that this would have removed the anomaly and that there is no voltage effect.

There is negligible uncertainty in the αc overlap correction for βd, since

$$\delta_{\beta d} = (0.16 + 0.64M) A_{\alpha c}/A_{\beta d} \ .$$

Including an NMR uncertainty of 0.1 MHz, and adding the corrections given in Sec. IV C, we find that βd yields

$$\Delta E - \mathcal{S} = 47\,844.27 \pm 0.28 \text{ MHz}.$$

Although βd results initially seemed to be of low quality, they have no unexplained power effect. Provided that the pressure and current extrapolation is correct, βd is the most credible of the three transitions that were studied.

H. Final Results

1. $\Delta E - \mathcal{S}$

The weighted average of the values for $\Delta E - \mathcal{S}$ obtained from αc and βd is 47 844.05 MHz and agrees with the βd result due to the larger uncertainty in αc. The difference from the extrapolated αc re-

TABLE VI. Observations on βd. This table gives the data of set 14. See Table IV for an explanation of column headings. The column labeled U gives a dimensionless coefficient (dependent on N_H and M) which relates shifts of the βd resonance to collisional quenching of the β state. Δ_{fit} is obtained from Eq. (8).

				Low power				High power			
Runs	N_H	P (mTorr)	I (mA)	M (W)	U	Δ_{raw} (MHz)	Δ_{fit} (MHz)	M (W)	U	Δ_{raw} (MHz)	Δ_{fit} (MHz)
545–56	5	10	4	0.06	0.70	3.50 ± 0.28	3.96	0.3	0.77	3.91 ± 0.14	4.39
557–62	5	10	2	0.1	0.71	2.14 ± 0.12	2.76	0.2	0.74	2.35 ± 0.17	2.89
563–70	5	10	1	0.1	0.71	2.02 ± 0.13	2.12	0.2	0.74	2.16 ± 0.29	2.23
571–81[a]	5	10	1	0.1	0.71	1.86 ± 0.26	2.12	0.2	0.74	2.40 ± 0.17	2.23
582–89[a]	5	19	1	0.1	0.71	2.52 ± 0.21	3.30	0.2	0.74	2.45 ± 0.12	3.45
590–97[a]	5	5	1	0.1	0.71	1.85 ± 0.24	1.47	0.2	0.74	1.18 ± 0.26	1.55
608–10	3	10	2	0.1	0.56	2.46 ± 0.08	2.35	0.5	0.58	2.83 ± 0.06	2.60
611–15	3	10	2	0.3	0.57	2.74 ± 0.04	2.47	0.8	0.59	3.20 ± 0.15	2.76
616–22	5	10	1	0.3	0.77	2.12 ± 0.23	2.35	0.8	0.88	2.65 ± 0.13	2.77
623–26	5	10	0.5	0.3	0.77	1.72 ± 0.16	2.02	0.8	0.88	2.25 ± 0.23	2.40
632–36	9	10	0.5	0.1	0.80	1.43 ± 0.20	1.92	0.8	1.0	2.16 ± 0.09	2.54
637–40	9	18	0.5	0.1	0.80	2.73 ± 0.16	2.85	0.8	1.0	4.18 ± 0.08	3.69
641[b]	9	18	1	0.1	0.80	3.69 ± 0.5	3.47	0.8	1.0	5.17 ± 0.5	4.47
643–50	9	26	1	0.1	0.80	4.54 ± 0.40	4.69	0.8	1.0	6.27 ± 0.19	5.98
651–55	9	5	1	0.1	0.80	1.56 ± 0.15	1.55	0.8	1.0	1.60 ± 0.11	2.06
656–57	9	5	0.5	0.1	0.80	2.29 ± 0.87	1.38	0.8	1.0	1.50 ± 0.58	1.85
682–84	9	5	1	0.1	0.80	1.56 + 0.13	1.55	0.8	1.0	1.68 ± 0.14	2.06
686–87[b]	9	2	1	0.1	0.80	1.47 ± 0.1	1.11	0.8	1.0	1.11 ± 0.1	1.51

[a]Bombarding voltage was 200 V rather than the usual 400 V.
[b]Uncertainty was fixed arbitrarily.

sult is 0.73 ± 0.51 MHz, which may not be statistically significant. However, since αc had an unexplained power shift, the presence of a systematic error is indicated. Thus the final uncertainty given below is taken as one-half the difference between the αc and βd results, $\sigma = 0.48$ MHz. This is felt to represent a "68% confidence interval" since 70% of the 24 αc observations lie within σ of 47 844.05 MHz and 96% lie within 2σ. Finally, we have

$$\Delta E - \mathcal{S} = 47\,844.05 \pm 0.48 \text{ MHz} ,$$

obtained from αc and βd.

2. $\mathcal{S}$

Using the TPL[1] value of α, one finds $\Delta E = 52\,027.78 \pm 0.21$ MHz. Subtracting the above result one obtains an indirect value for $\mathcal{S} = 4183.73 \pm 0.51$ MHz, adding the uncertainties in quadrature. The direct value obtained from αe was 4183.17 ± 0.54 MHz. Combining these two values, we obtain a final result

$$\mathcal{S} = 4183.45 \pm 0.52 \text{ MHz} .$$

3. *Comparison with Theory*

The calculation of ΔE is considered to be well understood. The main uncertainty in ΔE is due to the uncertainty in α, the fine-structure constant. The change in α^{-1} from the old value of 137.03876 to the TPL[1] value of 137.03602 raises ΔE by 2.07 MHz to 52 027.78 ± 0.21 MHz.[1] This change also raises $\mathcal{S}$ by 0.23 MHz. Using the results of Ref. 12, Erickson found $\mathcal{S} = 4183.11 \pm 0.60$ MHz. Including the results of Soto's analytic calculation for a fourth-order contribution,[21] Erickson found $\mathcal{S} = 4182.43 \pm 0.44$ MHz, the value given in Table I. Applequist and Brodsky[2] have made a computer calculation of this fourth-order contribution to $\mathcal{S}$ and obtained a different result from Soto's. Using the new α and their result, Applequist and Brodsky found $\mathcal{S} = 4184.4 \pm 0.5$ MHz. Our value of $\mathcal{S} = 4183.45 \pm 0.52$ MHz falls 0.9 ± 0.7 MHz lower than the Applequist and Brodsky value. (Uncertainties in $\mathcal{S}$ are "68% confidence" values. For the theoretical quotations, these uncertainties are taken as one-third of the author's "limit-of-error" uncertainty quotations.)

We conclude that there is little evidence of disagreement between the experimental and theoretical values of the level shift in the He^+ $n = 3$ case.

ACKNOWLEDGMENTS

The authors gratefully acknowledge the contributions of Professor Kenneth Lea, Dr. Stanley Kaufman, and Dr. Ralph Jacobs to the development of the apparatus. We have enjoyed many conversations with the above and also with Dr. William Wing during the course of the research.

APPENDIX: SHIFTS OF βd

Of the three transitions studied in this experiment

βd is the most susceptible to perturbing electric fields because it was unfortunately observed near the the βf crossing. For the purposes of this Appendix, we limit consideration to the three states β, d, and f. An electric field parallel to the magnetic field will couple β and f. A static field can shift the βd resonance in two ways. First, there is a Stark shift of the energy levels, and hence of the βd transition frequency. Second, because the βd resonance was not centered on the βf crossing, quenching of the β state through coupling with f will introduce an asymmetry into the βd resonance. This asymmetry results in a shift of the observed resonance.

Using the three-level treatment of Wilcox and Lamb,[22] it can be shown that quenching of the β state is twice as important, in this experiment, as the Stark effect in producing shifts of the βd resonance. In addition, time varying electric fields due to collisions with ions and atoms are thought to produce shifts of βd mainly through quenching and not through perturbation of energy levels. Thus we are primarily interested in estimating shifts due to quenching.

Purcell[23] has developed a theory for quenching of the metastable states of atomic hydrogen in the solar chromosphere. For a given perturber (electron or ion) of velocity v he finds a cross section, considering a single transition, proportional to $B^2 \ln(b_a/B)$, where $b_a = v/\omega$ is the adiabatic cutoff impact parameter and B is the impact parameter at which the probability of quenching becomes large. Here ω is the transition frequency. For his derivation Purcell required $B \ll b_a$. This condition is met in the present experiment for electron collisions, and a negligible cross section is found.

However, in the case of helium ions at relatively low temperatures, Purcell's theory is of marginal validity because $B \approx b_a$. In this situation, the notion of adiabaticity should be abandoned if there is appreciable decay of the short-lived state during the collision. Thus there is a need for a theory including decay that is applicable to low-velocity collisions. A static quenching theory[24] may be modified for quasistatic collisions if the interaction varies slowly enough and is weak enough. It is found that a $3S$ state coupled to a $3P$ state by a static electric field is quenched with an induced decay rate $\mu = 2V^2 \mathfrak{L}(\omega)/\hbar^2\gamma$, where γ is the average radiative decay constant of the $3S$ and $3P$ states and V is defined in Sec. II D. The magnetic field dependence of the $3S$ quenching is contained in the Lorentzian

$$\mathfrak{L} = \mathfrak{L}(\omega) = \gamma^2/(\omega^2 + \gamma^2) \ ,$$

where ω is the field-dependent transition frequency. The population P of the longer-lived $3S$ state obeys a rate equation with decay constant $\mu + \gamma_S$.

Going from the case of a static electric field to a slowly varying field, we have a time-dependent rate of induced decays $\mu(t)$. Supposing that the duration of a collision causing appreciable decay is shorter than the natural lifetime of the $3S$ state, $\tau_S = 1/\gamma_S$, the solution to the rate equation for the population is

$$P(t) = \exp\left[-\int_{-\infty}^{t} \mu(t')dt'\right] \ . \tag{A1}$$

It can be shown that one condition for the validity of the rate equation is $B \gg b_a$. Although this condition is not too well met, we will use the quasistatic theory because of its freedom from divergences.

For the purpose of this rough calculation, let us consider an ion with velocity v moving past an excited ion with a straight trajectory of impact parameter b and an orientation that produces a maximum electric field parallel to the magnetic field. Since the β state lives 30 times longer than the f state, we can calculate the β quenching from the interaction driving the βf transition:

$$V = e^2 z b (b^2 + v^2 t^2)^{-3/2} \ ,$$

where ez is the electric dipole matrix element for the βf transition. The probability of quenching is $1 - P(\infty)$ leading to a cross section of

$$\sigma_{\text{ion}} = 2\pi \int_0^\infty [1 - P(\infty)] b \, db$$

$$= 3\pi(\tfrac{1}{3})! \, \eta^{2/3} \ , \tag{A2}$$

where

$$\eta = 3\pi e^4 z^2 \mathfrak{L}/\hbar^2 v \gamma_P \ .$$

In a similar fashion, the quenching due to neutral atoms can be calculated. We use the dielectric constant ϵ and Loschmidt's number L to find the dipole moment induced on a single helium atom by an electric field. When such a field arises from an excited ion, the field back at the ion is

$$E = [(\epsilon - 1)/2\pi L] e/r^5 \ .$$

Using this field and the trajectory described previously, we find a quenching cross section due to atoms of

$$\sigma_{\text{atom}} = \tfrac{9}{7}\pi(\tfrac{7}{9})! \, \rho^{2/9} \ , \tag{A3}$$

where

$$\rho = 63(\epsilon - 1) e^4 z^2 \mathfrak{L}/128 L \hbar^2 v \gamma_P \ .$$

Limiting consideration to a single velocity, the quenching rate is

$$W = (\sigma_{\text{ion}} n_{\text{ion}} + \sigma_{\text{atom}} n_{\text{atom}}) v. \tag{A4}$$

The atom density is $3.5 \times 10^{13} P(\text{mTorr})$ atoms/cm^3. A model is needed to estimate the ion density. We assume that the only way for ions to escape from the interaction region is by moving along magnetic lines of force, since transverse motion will be in a circle of radius ≈ 0.01 cm at 4 kG. An upper limit on the effective area of the electron beam is obtained as 0.5 cm^2 from the area of the cathode and transmission of the grid. With an interaction

region 2.3 cm long and the ionization cross section for 400-V bombarding electrons given in Sec. IV A we find the number of ions/cm^3 is $9.6\times10^7 I(\text{mA})P$ (mTorr), if we take a velocity of 1.3×10^5 cm/sec along the magnetic lines of force. Using these densities the quasistatic theory yields a quenching rate of the β state equal to

$$W = x\mathfrak{L}^{2/9}P + y\mathfrak{L}^{2/3}PI \text{ MHz}, \quad \text{(A5)}$$

with x estimated as 0.047 and y as 0.026 when P is expressed in mTorr and I in mA. Since $\mathfrak{L}$ depends on the magnetic field and is centered at the βf crossing, 1 kG lower than the βd resonance, the quenching of the β state is greater on the low-field side of βd than on the high-field side. It is this asymmetric quenching which is the major cause of shifts of the observed βd resonance.

We now inquire what sort of shifts are expected from the quenching. Since the quenching rate W is small in comparison with the spontaneous decay rate γ_S, we may take $\gamma_a = \gamma_S + W$ for the β state wherever γ_a appears in the βd part of the lineshape expression [Eq. (5)] with which data is analyzed. Shifts due to quenching asymmetry can be expressed as a linear combination of atom and ion shifts in the following form:

$$\Delta = xU_P P + yU_{PI} PI\,. \quad \text{(A6)}$$

Here x and y are the factors appearing in Eq. (A5). U_P and U_{PI} are coefficients found numerically by taking W equal to $\mathfrak{L}^{2/9}$ or $\mathfrak{L}^{2/3}$, respectively, and analyzing certain representative runs to see how the value of Δ changes from the value obtained with $W=0$. It was found that U_P and U_{PI} were fortuitously nearly equal, so we may rewrite Eq. (A6) as

$$\Delta = U(xP + yPI)\,, \quad \text{(A7)}$$

where $U = U_P \simeq U_{PI}$. As shown in Table VI, U depends on the number and location of points taken on the resonance curve, and on the microwave power. This dependence was expected, since, for a given quenching asymmetry, the shift increases as the width of the resonance increases. Equation (A7) forms part of the modified extrapolation formula [Eq. (8)] which was used to fit the observed βd shifts. The fitting coefficients in Eq. (8), C_P and C_{PI}, are experimentally obtained values for the coefficients x and y appearing in Eq. (A7) and estimated in this Appendix. As discussed in Sec. IV G the estimates are $\frac{1}{2}$ to $\frac{1}{3}$ the size needed to fit the measurements.

Other mechanisms which have been considered are the microscopic static Holtsmark fields of ions and atoms, and the macroscopic fields of unneutralized charges. Even if it were not neutralized, the primary electron beam would be unimportant. However, on the basis of the above estimate of the ion density, we expect neutralization at pressures above 0.1 mTorr. Although the ion space charge could cause shifts $\approx 1(IP)^2$ MHz it is believed that enough slow electrons produced by secondary emission are trapped to largely neutralize it.

---

*Research sponsored by the Air Force Office of Scientific Research, under AFOSR Grant No. 249-67.

†Present address: Columbia Astrophysics Laboratory, Columbia University, New York, N. Y. 10027.

‡Present address: Bell Telephone Laboratories, Murray Hill, N. J.

[1]B. N. Taylor, W. H. Parker, and D. N. Langenberg, Rev. Mod. Phys. 41, 375 (1969), refered to as TPL in this paper.

[2]T. Applequist and S. J. Brodsky, Phys. Rev. Letters 24, 562 (1970).

[3]See Table I of Ref. 4.

[4]W. E. Lamb, Jr. and M. Skinner, Phys. Rev. 78, 539 (1950).

[5]E. Lipworth and R. Novick, Phys. Rev. 108, 1434 (1957).

[6]M. A. Narasimham, thesis (University of Colorado, 1968) (unpublished).

[7]M. Leventhal, K. R. Lea, and W. E. Lamb, Jr., Phys. Rev. Letters 15, 1013 (1965).

[8]D. L. Mader and M. Leventhal, Bull. Am. Phys. Soc. 13, 575 (1969).

[9]D. L. Mader and M. Leventhal, Bull. Am. Phys. Soc. 14, 942 (1969).

[10]W. E. Lamb, Jr. and T. M. Sanders, Jr., Phys. Rev. 119, 1901 (1960).

[11]R. R. Jacobs, K. R. Lea, and W. E. Lamb, Jr., Phys. Rev. A 3, 884 (1971); S. L. Kaufman, W. E. Lamb, Jr., K. R. Lea, and M. Leventhal, Phys. Rev. Letters 22, 507 (1969); and (to be published).

[12]G. W. Erickson and D. R. Yennie, Ann. Phys. (N. Y.) 35, 271 (1965).

[13]G. W. Erickson (private communication).

[14]H. A. Bethe and E. S. Salpeter, *Quantum Mechanics of One- and Two-Electron Atoms* (Springer, Berlin, 1957).

[15]D. T. Wilkinson and H. R. Crane, Phys. Rev. 130, 852 (1963).

[16]J. H. E. Mattauch, W. Thiele, and A. H. Wapstra, Nucl. Phys. 67, 1 (1965).

[17]J. W. DuMond, Ann. Phys. (N. Y.) 7, 365 (1959).

[18]H. S. W. Massey, *Handbuch der Physik*, edited by S. Flügge (Springer, Berlin, 1956), Vol. 36, p. 360.

[19]W. E. Lamb, Jr. (unpublished).

[20]L. Frampton and J. Alenen, Yale Computer Center Memorandum No. 71s, 1969 (unpublished).

[21]M. F. Soto, Jr., Phys. Rev. Letters 17, 1153 (1966).

[22]L. R. Wilcox and W. E. Lamb, Jr., Phys. Rev. 119, 1915 (1960).

[23]E. M. Purcell, Astrophys. J. 116, 457 (1952).

[24]W. E. Lamb, Jr. and R. C. Retherford, Phys. Rev. 79, 549 (1950).